ISSN 1027-5495. Functional Materials, 28, No.2 (2021), p. 386-393.
doi:https://doi.org/10.15407/fm28.02.386

In situ synthesis of Diatomite@BiOBr composites by a facile method and its application in visible-light-driven decomposition of rhodamine B

Jianhua Jiang, Gang Liao

Department of Traffic and Municipal Engineering, Sichuan College of Architectural Technology, 610399 Chengdu, China

Received November 11, 2020

Diatomite@BiOBr composites were fabricated by a facile method in this study. The crystalline phase, morphology, particle size distribution, pore structure, and optical properties were characterized by X-ray diffraction, scanning electron microscope, laser particle sizer, N_2 adsorption-desorption analysis, and UV-vis diffusion reflection spectra. Decomposition of rhodamine B under visible light ($\lambda > 400$ nm) was carried out to measure the photocatalytic activity of as-prepared composites. The results showed that the addition of diatomite can lead to the enhancement of photocatalytic activity of Diatomite@BiOBr composites, among which the composite with diatomite content of 40 % exhibited the highest photocatalytic activity up to 67.07 % within 50 min. This enhanced effect can be attributed to the fact that diatomite played the role of a platform, on which the BiOBr microsphere can evenly distribute increasing active sites, while diatomite can promote the separation of hole-electron pairs, thus enhancing the photocatalytic activity. Our findings may contribute to the use of natural porous mineral for the preparation highly efficient photocatalytic composites.

Keywords: BiOBr, diatomite, photo-decomposition, rhodamine B.

Синтез *in situ* композиту Diatomite@BiOBr простим методом і його застосування для розкладання родаміну B під дією видимого світла. *Jianhua Jiang, Gang Liao*

Композити Diatomite@BiOBr виготовлено простим методом і досліджено. Кристалічна фаза, морфологія, гранулометричний склад, структура пір і оптичні властивості охарактеризовано за допомогою дифракції рентгенівських променів, скануючого електронного мікроскопа, лазерного вимірювача розміру часток, адсорбційно-десорбційного аналізу N_2 і УФ-випромінювання, спектрів видимого дифузного віддзеркалення. Розкладання родаміну B під видимим світлом ($\lambda > 400$ нм) проводили для вимірювання фотокаталітичної активності композитів у свежевиготовленому вигляді. Результати показали, що додавання діатомиту може привести до посилення фотокаталітичної активності композитів Diatomite@BiOBr, серед яких композит з вмістом діатомиту 40 % проявив найвищу фотокаталітичну активність, досягнувши 67,07 % за 50 хв. Цей посилений ефект можна приписати тому, що діатомит грає роль платформи, на якій мікросфери BiOBr можуть рівномірно розподіляти активні центри, які збільшуються в той час як діатомит може сприяти розділенню пар дірка-електрон, тим самим збільшуючи фотокаталітичну активність. Наші результати можуть знайти застосування при використанні природного пористого мінералу для отримання високоефективних фотокаталітичних композитів.

Композиты Diatomite@BiOBr изготовлены простым методом и исследованы. Кристаллическая фаза, морфология, гранулометрический состав, структура пор и оптические свойства были охарактеризованы с помощью дифракции рентгеновских лучей, сканирующего электронного микроскопа, лазерного измерителя размера частиц, адсорбционно-десорбционного анализа N_2 и УФ-излучения, спектров видимого диффузного отражения. Разложение родамина B под видимым светом ($\lambda > 400$ нм) проводили для измерения фотокаталитической активности композитов в свежеприготовленном виде. Результаты показали, что добавление диатомита может привести к усилению фотокаталитической активности композитов Diatomite@BiOBr, среди которых композит с содержанием диатомита 40 % проявил наивысшую фотокаталитическую активность, достигнув 67,07 % за 50 мин. Этот усиленный эффект можно приписать тому, что диатомит играл роль платформы, на которой микросферы BiOBr могут равномерно распределять увеличивающиеся активные центры, в то время как диатомит может способствовать разделению пар дырка-электрон, тем самым увеличивая фотокаталитическую активность. Наши результаты могут способствовать использованию природного пористого минерала для получения высокоэффективных фотокаталитических композитов.

1. Introduction

In recent years, water pollution has become an urgent issue in modern society. The textile industry and relative industries are very significant pollution sources of aquatic environment, as about 60 % ~ 70 % of dyestuffs in the wastewater are toxic, which can lead to many diseases such as cancer [1–4]. Up to now, a number of technologies have been implemented to purify textile wastewater by filtering, adsorbing or decomposition of these dyestuffs [5–7]. Among the applied technologies, heterogeneous photocatalysis is considered one of the most promising solutions for eliminating water pollution, since the decomposition reaction is driven only by solar energy and the pollutants will be finally oxidized into water and carbon dioxide by active oxygen species (AOS) like hydroxyl radical (·OH) [8, 9]. So far, Titania has been the most-widely used photocatalyst, due to its high chemical stability, non-toxicity, and low price [10, 11]. However, the band gap (about 3.2 eV) of Titania is large, so, it can only be irradiated by UV-light ($\lambda < 380$ nm), which is only 4 % of solar radiation [12–14]; this limits the decomposition efficiency in practice. Therefore, the efforts of scientists around the world have been directed towards the development of an improved photocatalytic material with activity under visible light.

Recently, bismuth oxybromide (BiOBr), a novel semiconductor photocatalyst, has been found to exhibit high photocatalytic efficiency in wastewater treatment under visible light irradiation. However, the drawbacks of pure BiOBr, such as low specific area, a high recombination rate of hole-electron pairs, and poor dispersion also limit its applications. Thereby, several strategies have been proposed to overcome these disadvantages [15–17]. Immobilization of BiOBr on some catalyst supports, such as reduced graphene oxide [18], carbon nitride foam [19], montmorillonite [20], and flyash [21], has proven to be an effective approach to improve the photocatalytic performance of BiOBr. Diatomite, a natural mineral derived from the deposition of the skeletons of single celled algae, is mainly composed of amorphous SiO_2 [22]. It is a good carrier for photocatalysts, due to its specific properties, such as large specific surface areas, high chemical inertness, abundant resource and low cost [23]. Moreover, the previous research reported that the surface of diatomite is rich in hydroxyl groups, which can prevent electron-hole recombination by capturing holes, thus enhancing its photocatalytic activity [22]. So, it's reasonable to expect the remarkable photocatalytic properties of the diatomite@BiOBr hybrid. However, to our best knowledge, few researches on the diatomite@BiOBr composite have been reported at present.

Herein, we report a facile method to prepare diatomite@BiOBr composites. Different samples are synthesized by changing the ratio of BiOBr to diatomite. The decomposition of rhodamine B (RhB) is used to evaluate the photocatalytic activity of the as-prepared composite, because RhB is a recalcitrant dye commonly found in textile wastewater, which is difficult to remove by physical chemical treatments and biological oxidation [24]. Some important material characteristics of the composites including crystallinity, morphology, specific surface area, pore size distribution, and optical properties are measured to interpret the relationship between microstructure and photocatalytic efficiency.

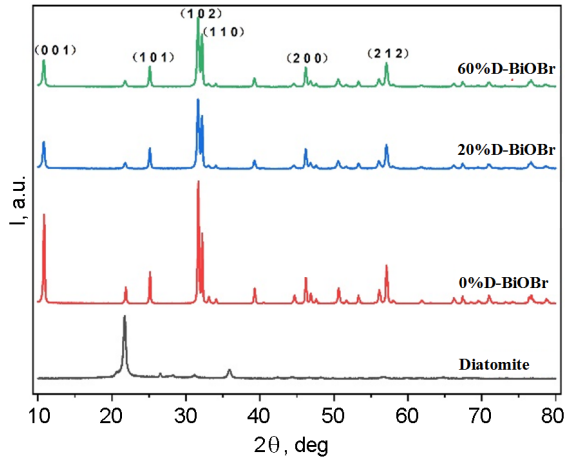

Fig. 1. X-ray diffraction patterns.

2. Experimental

2.1. Materials

All the chemical reagents were purchased from Shanghai Taitan Technology Co., Ltd. They were analytical reagents without further purification. Natural diatomite used in this study was provided by Sinopharm Chemical Reagent Co., Ltd. Diatomite was calcined at 105°C for 24 h, and the content of SiO2 in it exceeds 89 wt.%.

2.2. Preparation of samples

A certain amount of $Bi(NO_3)_3 \cdot 5H_2O$ was added into 25 ml ethylene glycol (EG), the solution was put in a 45°C water bath and then ultrasonically treated for 1 h until the $Bi(NO_3)_3 \cdot 5H_2O$ was totally dissolved; thus, the solution A was obtained. Then the stoichiometric amount of KBr and diatomite were added into 20 ml deionized water, and the mixture was stirred for 30 min (solution B). Afterwards, solution A was added dropwise to solution B with continuous stirring; then the mixture was kept without stirring for 2 h to realize the full precipitation of BiOBr on the surface of diatomite. The formed precipitate was centrifugated and washed by ethanol (1 time) and deionized water (2 times). Finally, the product was dried in an oven at 80°C for 12 h to obtain the diatomite@BiOBr composite. The contents of diatomite in these composites (wt. %) were 0, 20, 40, 60, and 80; and these samples were labelled as 0 %D–BiOBr, 20 %D–BiOBr, 40 %D–BiOBr, 60 %D–BiOBr, 80 %D–BiOBr, respectively.

2.3. Characterization

X-ray diffraction (XRD) studies were performed on an X-ray diffractometer (Rigaku D/max2550, Japan) with a CuKα X-ray source operating at 40 kV and 100 mA. The diffraction angles (2θ) between 10° and 80° were continuously recorded with the step of 0.02°. Morphology was studied by a scanning electron microscope (Hitachi TM4000 Plus, Japan) and the distribution of elements on a micro-area was recorded using energy disperse spectroscopy (IXRF, USA). All samples were observed in the backscattering mode of electrons without gold coating. The particle size distribution (PSD) in the samples was analyzed by a laser particle sizer (Beckman Coulter, LS 230, USA). Registration of UV-vis diffusion reflection spectra was performed with a powder sample using a spectrophotometer (Hitachi U-4100, Japan). The spectra were recorded at 300–800 nm and referred to $BaSO_4$. The BET specific surface area and pore size distribution were measured by a N_2 adsorption-desorption analyzer (Quantachrome Nova, USA).

2.4 Measurement of photocatalytic activity

Photocatalytic activities of diatomite@BiOBr composites were evaluated by decomposition of RhB (0.01 g/L) under visible light irradiation of a 500 W Xenon lamp with the 400 nm cutoff filters. Diatomite@BiOBr composite (0.05 g) and 50 ml of RhB aqueous solution were added into a Petri dish with 10 cm in diameter. Before irradiation, the Petri dish was put in a dark place with continuous stirring; then 2 ml of the RhB aqueous solution were fetched from the mixture using a pipette every 5 min (6 times in total). After switching on the Xenon lamp, 2 ml of the RhB aqueous solution were fetched every 10 min (5 times in total). All the RhB samples were centrifugated in a high-speed centrifuge at a speed of 7000 RCF for 3 min. And the absorbance of the RhB supernatant at a wavelength of 554 nm was measured by an UV-vis spectrophotometer (Meipuda UV1200, China).

2.5 Measurement of photocurrent

Transient photocurrent response was conducted in a standard three compartment cell with the 0.1 M Na_2SO_4 electrolyte and recorded on a CS310H Eelectrochemical workstation (CorrTest, China). Saturated calomel electrodes (SCE) and Pt slice were used as reference electrode and counter electrode, respectively. Diatomite@BiOBr composite was dispersed in Nafion solution and coated on indium tin oxide glass (ITO, 6 Ω, 10×10×1.1 mm), forming the working elec-

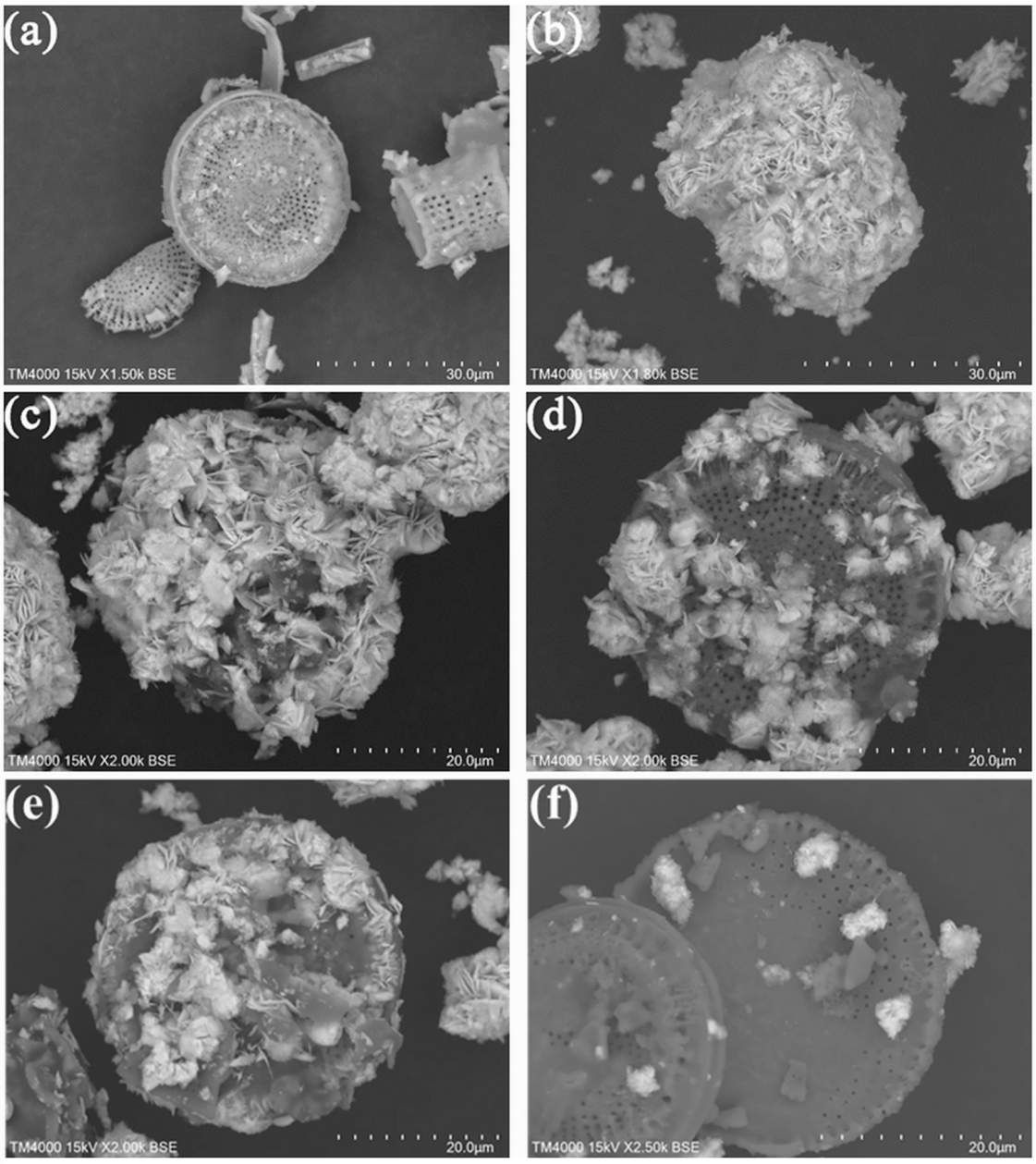

Fig. 2. SEM images: (a) Diatomite; (b) 0 %D–BiOBr; (c) 20 %D–BiOBr; (d) 40 %D–BiOBr; (e) 60 %D–BiOBr; (f) 80 %D–BiOBr.

trode. The electrochemical tests were measured at 0.5 V with a 500 W Xe lamp (a 400 nm cutoff filter was used) as the light source, and light on/off alternation was realized by a shutter every 20 s.

3. Results and discussion

3.1. XRD analysis

The X-ray diffraction patterns of diatomite@BiOBr composites are shown in Fig. 1. According to the JCPDS card No. 09-0393, diffraction peaks can be observed at 2θ of 10.900°, 25.157°, 31.692°, 32.220°, 46.208°, and 57.116°, which correspond to the crystal planes of (0 0 1), (1 0 1), (1 0 2), (1 1 0), (2 0 0), and (2 1 2) of BiOBr. For diatomite sample, the diffraction peak at $2\theta = 21.840°$ corresponds to the (1 0 1) crystal planes of cristobalite; this indicates that cristobalite was a symbiotic with diatomite used in this study [22]. Due to the amorphous form of diatomite, no diffraction peaks of diatomite phase were observed in all samples.

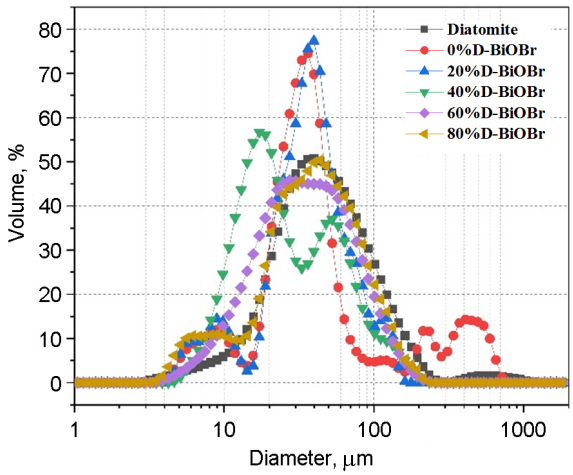

Fig. 3. Particle size distribution curves.

3.2. Morphology analysis

The morphology of the as-prepared composites is revealed by SEM. As shown in Fig. 2a, diatomite has a characteristic porous structure, and the pores are well associated with impurities removed by heat treatment. This pore structure is an ideal mass transfer channel for pollutans and has a large surface area, which allows it to be used as a sorbent for pollutant molecules and a carrier for photocatalysts. Fig. 2b depicts the SEM images of BiOBr. It can be seen that BiOBr presents flower-like microspheres with a diameter of 30 μm, which are self-assembled with nanosheets. Figs. 3c–f display the morphology of diatomite@BiOBr composites with different addition of BiOBr, respectively. Bi and Br elements found in the composite confirm that BiOBr was successfully deposited on diatomite. However, when the content of BiOBr was high (20% D–BiOBr), the surface of diatomite was completely covered with BiOBr nanosheets, which overlapped on each other, forming a dense shell. As a consequence, the pore structure of diatomite was blocked, which may be unfavorable for photocatalytic activity. By contrast, when the BiOBr content decreased (40 % D–BiOBr and 60% D–BiOBr), BiOBr was uniformly dispersed on the diatomite surface. The fact that BiOBr microspheres coexist with porous diatomite may cause a synergetic effect to enhance photocatalytic activity. When the BiOBr content was too low (80% D–BiOBr), only a few small BiOBr microspheres (about 5 μm) can be observed on the surface of diatomite.

3.3. Particle size distribution and specific surface area

Fig. 3 displays the particle size distribution of as-prepared samples. In general, three kinds of curves with different shapes were observed. At a small addition of diatomite, the samples with 0 % D–BiOBr and 20 % D–BiOBr had similar particle size distribution curves. The curves were sharp, and most of the particles were in the range of 30–40 μm, which is typical of BiOBr particles. This was because at the low diatomite content, most BiOBr nanosheets self-assembled into microspheres. When the diatomite content increased, the curve of 40 % D–BiOBr showed a bimodal distribution. This can be explained by the fact that a certain amount of BiOBr nanosheets was deposited on diatomite surface forming the diatomite@BiOBr composite, while another part of BiOBr was assembled into smaller BiOBr microspheres. With an increase in the diatomite content to 60 % and 80 %, the curves of the samples with 60 % D–BiOBr and 80 % D–BiOBr exhibited the properties of diatomite, because a small amount of BiOBr nanosheets interacts with diatomite, having an insignificant effect on the morphology of diatomite. From the above analysis, it can be concluded that with a suitable ratio of BiOBr/diatomite, diatomite plays the role of not only a carrier, but also a dispersing agent for BiOBr [25]. The BET specific surface area (S_{BET}), pore size, and pore volume data are presented in Table. It can be seen that S_{BET} of the sample with 0 % D–BiOBr was relatively low (1.629 m^2/g) compared

Table. Surface characteristics of pure Diatomite, 0 % D–BiOBr, and 40 % D–BiOBr samples

Sample	BET specific surface area, m^2/g[a]	Pore diameter, nm	Pore volume, cm^3/g[b]
Diatomite	17.125	12.564	0.059
0 % D–BiOBr	1.629	5.853	0.007
40 % D–BiOBr	3.436	6.034	0.009

[a]Specific surface area measured using multi-point BET method.

[b] Pore diameter calculated from the desorption isotherm of BJH model.

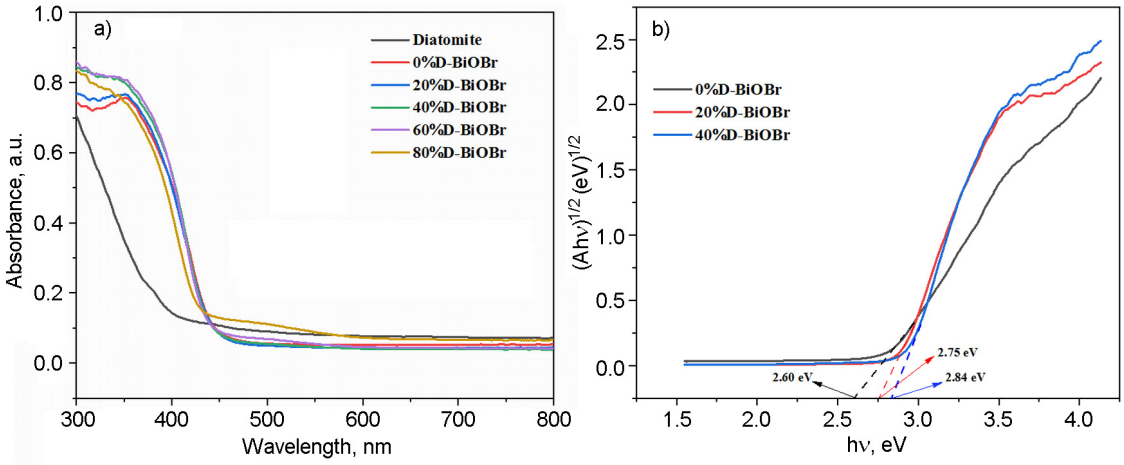

Fig. 4. UV-visible diffuse reflectance spectra.

to that of diatomite (17.125 m^2/g), which was in accordance with the results of SEM. After loading BiOBr onto diatomite, S_{BET} of the sample with 40 %D–BiOBr slightly increased to 3.436 m^2/g, indicating an improvement in the porosity of the composite. It has been proved that a large surface area with a mesoporous structure can facilitate adsorption, desorption and diffusion of reactants and products, so the composite prepared in this study may possess high photocatalytic activity.

3.4. UV-vis DRS analysis

The UV-visible diffuse reflectance spectra (DRS) of diatomite, 0 %D–BiOBr and 40 %D–BiOBr-composites are shown in Fig. 4. It can be seen that pristine BiOBr and Diatomite@BiOBr composites showed the excellent absorption when irradiated with visible light, the absorption edge of which was about 460 nm, while the absorption edge of diatomite was only 380 nm. For semiconductors, the band gap is closely related to optical transitions, and generally the band gap of a semiconductor could be calculated by the Kubelka-Munk function:

$$\alpha h\gamma = A(h\gamma - E_g)^{n/2}, \quad (1)$$

where α is the absorption coefficient, h is Planck's constant, γ is the light frequency, A is the measured absorbance, E_g is the energy difference between the conduction and valence bands, and $n = 4$ (for an indirect transition in BiOBr).

The estimated band gap values for the 0 %D–BiOBr, 2 %D–BiOBr, and 40 %D–BiOBr samples were 2.60 eV, 2.75 eV, and 2.84 eV, respectively. Although the band

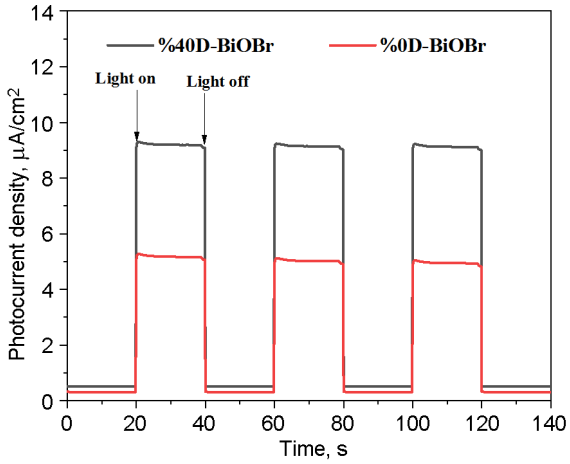

Fig. 5. Transient photocurrent responses of 0 %D–BiOBr and 40 %D–BiOBr samples at 0.5 V under visible light.

gap value of the diatomite@BiOBr composites was a little higher than that of pure BiOBr, the diatomite@BiOBr composites still held the ability to absorb visible light.

3.5. Photocurrent analysis

Fig. 5 presents the transient photocurrent responses of 0 %D–BiOBr and 40 %D–BiOBr samples. It can be seen that both samples quickly exhibited photocurrent response when the light was turned on. The photocurrent density of the 0 %D–BiOBr sample is about 5.1 $\mu A/cm^2$, which is much lower than that of the 40 %D–BiOBr sample (9.2 $\mu A/cm^2$). In other words, the hole-electron separation efficiency of the 40 %D–BiOBrD-composite was almost 1.8 times higher than that of the 0 %D–BiOBr sample. This may be attributed to the fact that hydroxyl groups existing on the surface of diatomite act as hole captures, improving

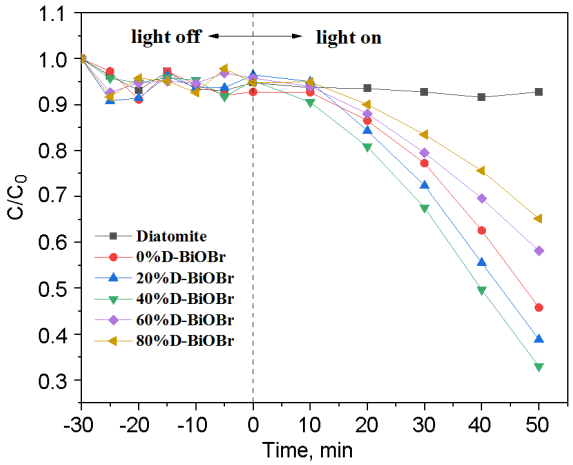

Fig. 6. (a) The RhB photocatalytic decomposition rate.

the hole-electron separation and preventing its recombination [26]. The result demonstrates that diat omite has a positive effect on the separation of phot ogenerated charge carriers and an increase in photocatalytic efficiency [27].

3.6 Photocatalytic activity

The results of RhB photocatalytic degradation over as-prepared composites are shown in fig. 6. Before illumination, the concentration of RhB decreased a little for all samples. And upon switching light on, RhB concentration declined immediately, except for diatomite sample. This indicates that diatomite had no photocatalytic activity and can only remove RhB molecules by physical adsorption. The degradation tendency of RhB over all Diatomite@BiOBr composites were similar with each other. The RhB degradation rate rose with the diatomite to BiOBr ratio (below 40%), however, when the diatomite content exceeded 40%, RhB degradation efficiency decreased dramatically with the diatomite content. Among these samples, 40% D-BiOBr had the highest degradation efficiency and 67.07% of RhB can be removed within 50 min. It can be found that the photocatalytic reaction complied with the pseudo-first-order rate law during the irradiation process. The reaction rate constants were 0.00013, 0.00317, 0.00371, 0.00752, 0.00279, and 0.00140 for the diatomite@BiOBr composites with diatomite contents of 100 %, 0 %, 20 %, 40 %, 60 %, and 80 %. Namely, the photocatalytic activity of the 40 % D–BiOBr sample was highest, which was almost 2.37 and 5.37 times higher than of that of pure diatomite and 80 % D–BiOBr, respectively. This is because nano-sheet units of BiOBr overlapped with each other, which will reduce the photon absorption efficiency, therefore, the photocatalytic efficiency was restricted. Although BiOBr can be activated by visible light, the photocatalytic activity of pure BiOBr was still limited by geometry effect. After loading BiOBr on diatomite, this limitation of geometry effect was alleviated, as diatomite has a high specific surface area and can provide a porous framework for supporting BiOBr. At the diatomite content of 40%, the aggregation of BiOBr nano-sheets will be hindered, as a result BiOBr can be evenly distributed on the surface of diatomite, thus providing more photocatalytic active sites and promoting the separation of hole-electron pairs. When diatomite content was too high, despite the highly homogenous dispersion of BiOBr, the photocatalytic activity maintained low, due to the low BiOBr content and small quantity of active sites.

According to the character of RhB decomposition, the process of RhB photocatalytic decomposition on the diatomite@BiOBr composites can be divided into several steps. Firstly, RhB molecules can freely migrate to the pore structure of diatomite from the aqueous environment, because the RhB molecule size is about 1.59×1.18×0.56 nm, which is smaller than the average pore diameter of the diatomite@BiOBr composite. Due to the large specific surface area, the adsorption equilibrium is established in a short time and RhB molecules can be trapped in the cavities and external surfaces of diatomite, so, the concentration of RhB around BiOBr remained high. As soon as the BiOBr microspheres are illuminated by visible light, electron-hole pairs will be generated on the BiOBr surface, which will react with G2OH- and the dissolved O_2 in the aqueous solution to form ROS, such as hydroxide radicals (·F2OH), superoxide radicals (O_2^-) and hydrogen peroxide (H_2O_2) in different chain reactions. RhB will be oxidized to inor ganic substances by hydroxide radicals (·OH) as shown in Eq. 2 [28]:

$$C_{28}H_{31}ClN_2O_3 + \cdot OH \rightarrow CO_2 + H_2O. \quad (2)$$

When the adsorbed RhB were decomposed by hydroxide radicals (?OH), the adsorption equilibrium was broken, and more RhB molecules would be captured by diatomite@BiOBr composite and then more RhB would be degraded.

4. Conclusions

To summarize, we proposed a facile method to synthesize diatomite supported BiOBr composites. By changing the addition of diatomite, it is possible to ensure that the BiOBr microspheres are evenly distributed on the diatomite framework, and the photocatalytic activity can also be regulated. Experiments on photo-decomposition of RhB proved that the 40 %D–BiOBr composite provides the highest photocatalytic activity, far superior to that of the pure BiOBr. Diatomite can not only depress the agglomeration of BiOBr increasing the active sites, but also acts as an excellent carrier for the separation and fast transfer of photogenerated electrons. Our research may promote the application of natural mineral in improving the photocatalytic performance of photocatalytic composites.

Acknowledgements. This research was funded by Deyang Science and Technology Program (Nos. 2020SZZ047 and 2019SZ083).

References

1. Z.Sun, Z.Hu, Y.Yan, S.Zheng, *Appl. Surf. Sci.*, **314**, 251 (2014).
2. A.Luengas, A.Barona, C.Hort et al., *Rev. Environ. Sci. Bio.*, **14**, 499 (2015).
3. R.O.Alves de Lima, A.P.Bazo, D.M.F.Salvadori et al., *Mutat. Res. Genet. Toxicol. Environ. Mutagen.*, **626**, 53 (2007).
4. T.Yahagi, M.Degawa, Y.Seino et al., *Cancer. Lett.*, **1**, 91 (1975).
5. M.R.Gadekar, M.M.Ahammed, *J. Environ. Manage.*, **231**, 241 (2019).
6. G.Crini, G.Torri, E.Lichtfouse et al., *Environ. Chem. Lett.*, **17**, 1645 (2019).
7. S.K.Padmanabhan, S.Pal, E.Ul Haq, A.Licciulli, *Appl. Catal. A Gen.*, **485**, 157 (2014).
8. M.R.Hoffmann, S.T.Martin, W.Choi, D.W.Bahnemann, *Chem. Rev.*, **95**, 69 (1995).
9. D.He, H.Zhong, C.Gao, *J. Alloys Compd.*, **799**, 50 (2019).
10. C.McCullagh, N.Skillen, M.Adams, P.K.J.Robertson, *J. Chem. Technol. Biotechnol.*, **86**, 1002 (2011).
11. S.Pal, A.M.Laera, A.Licciulli et al., *Ind. Eng. Chem. Res.*, **53**, 7931 (2014).
12. S.Zheng, W.Jiang, Y.Cai et al., *Catal. Today*, **224**, 83 (2014).
13. T.Wu, P.Niu, Y.Yang et al., *Adv. Funct. Mater.*, **29**, 1901943 (2019).
14. Q.Guo, C.Zhou, Z.Ma, X.Yang, *Adv. Mater.*, **31**, 1901997 (2019).
15. M.Gao, D.Zhang, X.Pu et al., *Sep. Purif. Technol.*, **154**, 211 (2015).
16. Z.Liu, B.Wu, Y.Zhao et al., *Ceram. Int.*, **40**, 5597 (2014).
17. C.Xue, J.Xia, T.Wang et al., *Mater. Lett.*, **133**, 274 (2014).
18. S.Vadivel, P.Keerthi, M.Vanitha et al., *Mater. Lett.*, **128**, 287 (2014).
19. G.Cao, Z.Liu, *Mater. Lett.*, **202**, 32 (2017).
20. C.Xu, H.Wu, F.L.Gu, *J. Hazard. Mater.*, **275**, 18 (2014).
21. L.Lin, M.Huang, L.Long, D.Chen, *J. Alloys Compd.*, **615**, 929 (2014).
22. S.E.Ivanov, A.V.Belyakov, *Glass and Ceram.*, **65**, 48 (2008).
23. B.Wang, F.C.de Godoi, Z.Sun et al., *J. Colloid Interface Sci.*, **438**, 204 (2015).
24. M.Ge, N.Zhu, Y.Zhao et al., *Ind. Eng. Chem. Res.*, **51**, 5167 (2012).
25. Z.Jia, T.Li, Z.Zheng et al., *Chem. Eng. J.*, **380**, 122422 (2019).
26. B.Li, H.Huang, Y.Guo, Y.Zhang, *Appl. Surf. Sci.*, **353**, 1179 (2015).
27. H.Huang, X.Li, J.Wang et al., *ACS Catalysis*, **5**, 4094 (2015).
28. Y.Wang, Q.Yang, X.Wang et al., *Mater. Sci. Eng. B Solid State Mater. Adv. Technol.*, **244**, 12 (2019).